Structures 73 (2025) 108329

Contents lists available at ScienceDirect

Structures

journal homepage: www.elsevier.com/locate/structures

Machine learning assisted axial strength prediction models for concrete filled stainless steel tubular columns

Deeptarka Roy [a], Debarshi Das [a], Kamrul Islam [b], AHM Muntasir Billah [a,*]

[a] Department of Civil Engineering, University of Calgary, Calgary, AB T2N 1N4, Canada
[b] Department of Civil, Geological and Mining Engineering, Polytechnique Montreal, Montreal, QC, Canada

ARTICLE INFO

Keywords:
CFSST column
Axial capacity
Machine learning
Explainable
SHAP
CatBoost

ABSTRACT

Concrete filled stainless steel tubular (CFSST) columns have gained popularity over conventional concrete filled steel tubular (CFST) columns owing to their higher axial capacity and excellent corrosion resistance of stainless steel (SS). Numerous experimental and numerical research have been performed to evaluate CFSST column response under different loading scenarios. Despite all these studies, inaccuracy still exists in predicting the axial strength of CFSST columns. Moreover, unique properties of SS do not allow using conventional code equations developed for CFST columns to be used for axial strength prediction of CFSST columns. To this end, this study aims to develop data-driven machine learning (ML) techniques for predicting the axial capacity of CFSST columns. A comprehensive dataset of 422 circular and rectangular CFSST columns are carefully gathered from literature, which is employed for developing the data-driven ML models. Model accuracy is assessed using various performance metrics such as coefficient of determination (R^2), root mean square error (*RMSE*), mean absolute error (*MAE*), Nash-Sutcliffe Model (*NSE*) and Index of Agreement (*d*). Out of the ten ML algorithms considered in this study, CatBoost (CatB) turns out to be the most accurate one. SHapley Additive exPlanations (SHAP) analysis is performed to interpret the outcomes of the ML model and explain the importance of each input feature. The best performing CatB model is compared with six different design code equations to showcase its acceptance and superior performance. It is observed that the ML model provides a quick and accurate estimate of the axial capacity of CFSST columns by overcoming the limitations of existing design codes. For identifying the resistance factor for the CatB model, reliability analysis is also performed following AISC 360–16 provision. Finally, an interactive graphical user interface is developed for practicing engineers to enhance the accuracy of CFSST axial capacity prediction while promoting the use of interpretable ML models.

1. Introduction and background

Stainless steel (SS) has grown in popularity in the construction sector over the past several years. This can be attributed to the higher durability [1] of SS combined with improved corrosion [1] and fire [2] resistance and offers enhanced strength in contrast to carbon steel [3]. Despite having several benefits, the application of SS has been quite restricted due to its high initial cost. An efficient method to offset SS's higher cost is to fill the hollow tube with concrete to combine the benefits of steel and concrete as a composite. As a result, the member's load carrying capability is increased and its production cost is decreased [4].

In the past decade, there has been an increasing trend in utilizing concrete filled stainless steel tubular (CFSST) columns in civil engineering applications. Compared to conventional regular carbon steel (CFST) columns, the CFSST columns possess higher load carrying capacity owing to the superior material properties of stainless steel [5]. Carbon steel exhibits a linear elastic region and a yield point followed by a yield plateau whereas stainless steel exhibits nonlinear ductile material response with higher level of strain hardening and thus leading to CFSST columns with more ductile behavior than their CFST counterpart [6]. These advantages of CFSST columns have attracted researchers to carry out experimental as well as numerical investigations [4–7].Despite having high initial cost, CFSST columns are beneficial when the life cycle cost of the whole project is considered. This is accredited to the fact that resistance against corrosion for stainless steel is significantly better than carbon steel. CFSST columns require little to no maintenance

* Corresponding author.
E-mail addresses: deeptarka.roy@ucalgary.ca (D. Roy), debarshi.das@ucalgary.ca (D. Das), kamrul.islam@polymtl.ca (K. Islam), muntasir.billah@ucalgary.ca (A.M. Billah).

https://doi.org/10.1016/j.istruc.2025.108329
Received 30 July 2024; Received in revised form 20 January 2025; Accepted 28 January 2025
Available online 5 February 2025

during the whole service life in comparison to the CFST column where regular maintenance such as spray of anti-corrosive coatings on outer surface is essential over the service life. Furthermore, they are aesthetic and the column size can be further reduced due to the enhanced strength as compared to conventional CFST columns [8]. Since carbon steel and SS have different mechanical properties, the confinement effect and the deformation response of CFSST columns are dissimilar from its CFST counterpart [9]. There are various parameters including length (L), height (H), thickness of the tube (t), characteristics strength of concrete (f_c'), ultimate strength of steel (f_u) amongst others that govern the axial strength of CFSST columns. The current design codes are conservative while assessing the axial capacities of CFSST columns since they don't consider stainless steel properties for strength calculation. Consequently, it's critical to develop a comprehensive framework for accurate axial capacity prediction of CFSST columns.

1.1. Prior research on CFSST columns

Numerous experimental and numerical investigations have been conducted over the past 20 years to examine the behavior of CFSST columns. Uy et al. [4] tested 117 specimens of short and slender CFSST columns to assess their performance under axial loading. When compared with different codes such as AS 5100 [10], AISC 360–16 [11], DBJ/T [12] and EC4 [13], they found the axial capacities estimated using code provisions are conservative by an average of about (11−25)%.The predictions for circular columns were more conservative than those of square and rectangular counterparts. He and Zhao [14] tested 15 partially loaded and 3 fully loaded specimens to study the axial load carrying capacity of circular CFSST columns. The axial capacities acquired though experiments were compared with axial capacities obtained using different design codes EC4 [13] and AISC 360–16 [11]. The two design standards led to conservative results compared to the experimentally obtained axial capacity. The mean value of the ratios between experimental axial capacity and that predicted by EC4 [13] was 1.60 and the coefficient of variation (COV) was 0.23. The mean and COV between experimental and that predicted by AISC 360–16 [11] was 3.54 and 0.51 respectively. He et al. [6] conducted experimental and numerical investigation into the compressive strength and load carrying capacities of concrete filled high-chromium stainless steel tube (CFHSST) stub columns. Since, there is no established design provisions for CFHSST columns, the experimental results were compared with code equations for CFST columns. The comparison depicted that AISC 360–16 [11] and EC4 [13] were both conservative while predicting the compressive strength. The mean value of ratios between experimental and predicted strength for AISC 360–16 [11] was 1.155 and for EC4 [13] was 1.087. The COV was 0.043 and 0.044 for AISC [11] and EC 4 [13], respectively. Lam and Gardner [15] experimentally investigated the behavior of concrete-filled circular and square sections consisting of regular as well as stainless steel under axial compression. The concrete cube strengths used in the experimental study ranged from 30 to 100 MPa. They found that the columns with stainless steel tubes and lower concrete strength depicted more ductile behavior as compared to the regular columns. The test results were compared with code provisions of EC4 [13] and ACI 318 [16] and found to be overly conservative specially for circular columns. The mean value of the ratios between experimental capacity and that predicted by ACI 318 [16] for circular stainless steel columns was 1.11 and the coefficient of variation (COV) was 0.07. The mean and COV between experimental and that predicted by EC4 [13] was 1.46 and 0.08, respectively. Young and Ellobody [17] performed experiments on concrete filled cold formed SS tubes with yield strength of 536 MPa and ultimate strength of 961 MPa. The concrete strength varied from 40 to 80 MPa, while the SS used were equivalent to EN 1.4462 and UNS S31803. The results were compared with the ACI 318–95 [16]) standard. The axial capacity values obtained using code equations were conservative as mean of the ratios between experimental capacity and that predicted by ACI 318–95 [16] was 1.01 and the coefficient of variation (COV) was 0.058. In a study by He et al. [18], the flexural buckling behavior and resistance of circular recycled aggregate concrete filled steel tubular columns (RACFFST) were analyzed based on the results obtained from experiments and numerical modeling. The results were compared with different codes. The assessment indicated that the design guidelines as specified by AS/NZS 2327 [19] standard resulted in unconservative prediction of flexural buckling resistance whereas the EC4 [13] standard yielded conservative results with an acceptable level of accuracy. The mean value of the ratios between experimental capacity and that predicted by AS/ZNS 2327 [19] was 0.87and the coefficient of variation (COV) was 0.08. The mean and COV between experimental and that predicted by EC4 [13] was 1.00 and 0.07, respectively.

Dai et al. [20] experimentally studied the axial behavior of 18 specimens which included 9 austenitic CFSST columns and 9 duplex CFSST Columns under compression. Finite Element (FE) models were also developed, which helped generate a wider range of data and finding the influence of different parameters on the strength of column. It was found that the European (EC4 [13]) and Chinese Code (GB 50936 [21]) underestimated the axial resistance of CFSST columns. Hence, new calculation methods were developed to provide enhanced strength predictions for austenitic as well as duplex CFSST columns. Guo et al. [22] and Li et al. [23] also proposed formulations for estimating the axial load carrying capacity of SS tubular stub columns.

Han et al. [8] presented a comprehensive review on the performance of CFSST column under different loading conditions. It was concluded that CFSST columns showed improved ductility, higher energy dissipation capacity and superior fire performance as compared to regular carbon steel. But the bond strength between a stainless steel and core concrete was lower for a CFSST column than a regular CFST column due to a smoother surface of stainless steel. The existing code equations of CFST columns such as AISC 360–16 [11], DB/J [12] and EC4 [13] underestimated the load carrying capacity for CFSST columns. This was accredited to the fact that strain hardening characteristics for stainless steel was not considered in the equations. Patel et al. [24] developed a fiber based column model for nonlinear analysis of axially loaded CFSST short columns. The model predicted load-strain behavior and ultimate bearing capacity with noteworthy accuracy when compared with experimental results. It was also observed that the design code equations such as ACI 318–95 [16] and EC 4 [13] was highly conservative in predicting the ultimate axial capacity of CFSST columns as they didn't take into account concrete confinement as well as strain hardening characteristics of stainless steel. Ding et al. [25] developed a 3D finite element model to study the behavior of CFSST stub columns. The finite element results revealed that there was increase in the ultimate bearing capacity of CFSST columns from its CFST counterpart as the concrete confinement effect was stronger for CFSST. Tam et al. [26] conducted an experimental program to investigate the behavior of recycled aggregate concrete filled stainless steel tubular (RACFSST) columns. For comparison purposes, reference specimens with carbon steel were also tested. Finite element analysis was also conducted and validated with experimental results. It was inferred that the replacement of normal concrete with recycled aggregate had relatively more influence on the strength of stainless-steel columns than that of carbon steel specimens. RACFSST columns also had higher residual strength than the counterpart with carbon steel. The FE models provided satisfactory results for both RACFSST and regular CFST columns.

The above-mentioned studies show that different axial capacity prediction models require different input parameters, and their values vary considerably. To counteract the uncertainties, a data-driven model can be a suitable approach for predicting the capacity considering the wide range of available datasets. Machine Learning (ML) is an advanced Artificial Intelligence (AI) technique that helps engineers explore a wide range of design possibilities and take decisions based on data-driven recommendations [27,28]. ML can be broadly grouped into different categories on the basis of nature of available input and desired output

(regression, classification, etc.). Moreover, the performance of the models can be assessed through evaluation matrices. Using ML models, it is possible to avoid costly, time-consuming experimental work as well as complex Finite Element (FE) simulations.

A wide range of data-driven applications have been demonstrated, for instance, prediction of material properties such as concrete strengths [29] and modulus of elasticity [30], compression capacity prediction of gusset plates [31], failure mode identification of columns [32], steel column-base connections [33], shear strength prediction of beam-column connections [34] and so on. Considerable research has also been done on predicting the axial capacity of conventional CFST columns [35],[36],[37],[38]. Hou and Zhou [36] developed a comprehensive dataset of circular CFST columns under axial load through literature survey. Different algorithms such as back-propagation neural network (BPNN), radical basis function neural network (RBPNN), gaussian process regressor (GPR) and multiple linear regression (MLR) were trained and tested on the given dataset. The developed ML models were compared with different design codes such as AISC-360 [11] and EC-4 [13]. It was observed that the models specially GPR predicted the axial capacity with higher accuracies than existing design standards. The R^2 value for GPR was 0.999 whereas that for AISC and EC 4, it was 0.765 and 0.644, respectively. Vu et al. [37] proposed a framework for predicting CFST axial capacity based on gradient tree boosting (GTB) algorithm, a powerful ML technique. The efficiency of the framework was compared with other ML algorithms such as support vector machines (SVM), decision tree (DT) and random forest (RF). Two different comparison metrics such as coefficient of determination (R^2) and mean square error (*MSE*) were calculated. The R^2 value for the GTB model was found to be 0.998, indicating model's high accuracy. Lee et al. [38] applied categorical gradient boosting (CATBoost) algorithm for predicting the axial capacity of CFST columns. The dataset was segregated into training, testing and 10-fold cross validation set. The axial capacities obtained from 10-fold cross validations were compared with different design codes (AISC 360–16, Eurocode 4 and AS/NZS 2327). The CATBoost model provided the highest accuracy compared to the design codes with R^2 value of 0.996.

1.2. Scope and objectives

Although sufficient research using ML has been done on CFST columns, data-driven prediction models for CFSST columns are currently absent in the literature. As reported in earlier studies, the codified equations for predicting the axial capacity of CFSST columns are conservative and fail to predict the axial capacity accurately. Furthermore, in the equations used for conventional CFST columns, stainless steel's strain hardening behavior is not considered, which is an important feature for CFSST columns. This paper focuses on developing a robust model to decrease prediction errors and overcome the limitations of current design equations. The objectives of this study include: (i) developing a large and comprehensive database from open literature, (ii) identifying the most important parameters influencing the axial capacity of CFSST columns, (iii) comparing the accuracy of the developed ML models with existing design codes, (iv) explaining the predicted results in relation to the input parameters employing Shapley Additive exPlanations (SHAP), (v) identifying the reliability of the best performed ML model in predicting CFSST axial capacity, and (vi) developing a Graphical User Interface (GUI) tool to benefit design engineers and researchers for CFSST column design and compressive capacity estimation.

2. Database for CFSST columns axial strength prediction

Establishing reliable prediction models and determining the critical parameters impacting prediction accuracy require a comprehensive database. A total of 211 datasets for circular and 211 datasets for rectangular CFSST columns reported in different peer-reviewed journals and dissertations are assembled in this study. Although the dataset (422) is not exhaustive, many past studies have successfully implemented various ML models using smaller datasets. Rahman et al. [31] used 250 datasets to develop high performance ML models for predicting the compressive capacity of gusset plate connections. Naderpour et al. [32] developed prediction models using Artificial Neural Network (ANN) and Decision Tree (DT) to identify failure modes in reinforced concrete columns using 163 datasets. Kabir et al. [33] utilized 189 experimental results for rapid identification of failure modes of column base plate connections using data-driven ML models. Although, it is possible to generate more synthetic data using FE simulation, the collected dataset is adequate for developing reliable ML models which is further justified by the accuracy and reliability of the obtained results.

With axial compression as the output (*N_Test*, kN), input characteristics that are utilized to create the ML models consist of the grade of stainless steel (*Grade SS*), length of the column (*L*, mm), thickness of the tube (*t*, mm), proof stress of stainless steel ($\sigma_{-0.2}$, MPa), ultimate strength of stainless steel (f_u, MPa), stainless steel elastic modulus (E_o, MPa), strain hardening component (*n*), compressive strength of concrete (f_c', Mpa), column diameter (*D*, mm) for circular section, width (*B*, mm) and height of cross-section (*H*, mm) for rectangular columns. The relative slenderness is expressed as *L/D* or *L/B* depending on the type of cross-section. An overview of the different parameters with their corresponding mean values along with the ranges are presented in Table 1.

Previous research involving data-driven ML models for CFST columns showed that sectional dimensions such as *D* or *B, t, L* significantly influence the axial capacity [36–38]. However, as discussed earlier, studies involving data-driven approach for CFSST columns are scarce in literature. Hence, to describe the feature importance in strength prediction, correlation analysis is carried out. One statistical technique that can quantify the relationship between two variables is correlation analysis. The Pearson correlation coefficient (*r*) is close to 1 when there is a strong positive correlation, close to 0 when a weak correlation is obtained and near −1 when a strong negative correlation is reflected. The correlation between different parameters for circular and rectangular sections are represented in the form of a correlation matrix (heatmap) in Fig. 1. For circular sections, *t* is the most important feature with *r* value of 0.85. *D* and *L* are the second most important features, with *r* values of 0.84. For rectangular sections, *t* is also the governing feature with a correlation coefficient of 0.86. The second and third most noteworthy parameters are *H* and *B* with *r* values being 0.73 and 0.66, respectively.

3. Development of ML models

Ten different ML models are developed and compared to predict the axial capacity of CFSST Columns. The assessment is performed using Python programming language and Scikit-Learn [39]. Scikit-Learn is a python library through which different ML models for regression,

Table 1
Mean and Range for Input Parameters.

Input Features	Circular Columns		Rectangular Columns	
	Mean	Range	Mean	Range
D (mm)	134.22	50.80–325.00	-	-
t (mm)	3.48	1.20–11.94	3.84	1.81–12.21
H (mm)	-	-	120.87	51–250
B (mm)	-	-	124.67	51–250
L (mm)	399.94	150–975	377.59	150–700
L/B	-	-	3.16	1.5–6.00
L/D	2.83	2.49–6.02	-	-
E_o (MPa)	193900	171900–206000	199730.05	172300–206100
$\sigma_{-0.2}$ (MPa)	225.70	200–444	433.11	211–581
f_u (MPa)	639	536–721	674.71	409–832
n	5.12	3.13–9.10	5.48	1.79–8.20
f_c' (MPa)	53.13	20.00–144.40	48.14	20.53–154.10

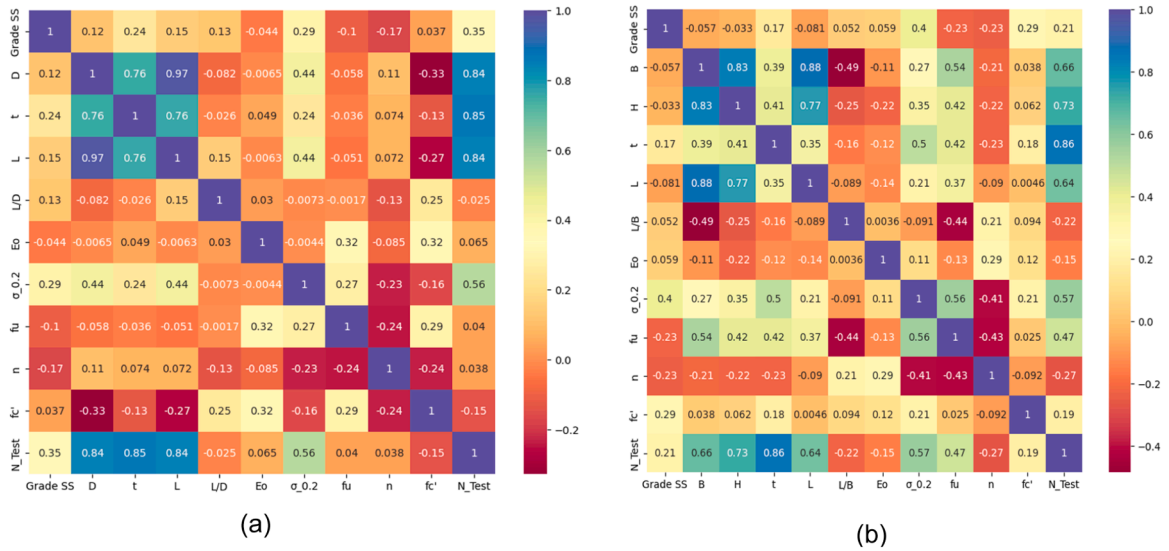

Fig. 1. Correlation matrix for **(a)** circular and **(b)** rectangular CFSST columns.

classification, clustering etc. are implemented. Ridge Regression (RR), Linear Regression (LR), Decision Tree (DT), Lasso Regression (LASSO), K-Nearest Neighbor (KNN), Random Forest (RF), Support Vector Machine (SVR), CatBoost (CatB), AdaBoost (AdaB) and XGBoost (XGB) are the models used in this study. LR [40] is one of the basic ML algorithms where the dependent variable (output) and independent variables (input) are modelled as a linear equation. RR [41] and LASSO [42] are improved regression algorithms where the optimization function known as the cost function are modified based on an optimization coefficient. The primary distinction between these two models is that, while RR takes the square of the coefficient, LASSO takes on the magnitude of the regression coefficients. In DT [43], the model is built in the form of a tree structure with decision nodes and leaf nodes. Leaf nodes hold the final output of the algorithm. RF [44] combines multiple decision trees to reduce overfitting of the dataset and provide better results. KNN [45] regression computes output in an intuitive manner by averaging the outcome in the same neighborhood. SVR [46] is one of the robust supervised learning models where a hyper plane is constructed to achieve separation by defining the largest distance to the nearest data point. XGB is a decision tree-based algorithm where gradient descent is used to minimize the cost function. AdaB is a regression model that uses adaptive boosting feature for performance improvement by integrating weak learning algorithms. CatB has two main features, categorical data (Cat) and gradient boosting (Boost) [47]. By this process, decision trees are built iteratively. So, subsequent tree influences the result of previous tree which leads to better predictions.

In this study, the entire dataset is divided into two sets, i.e., training and testing sets. The training set consists of 80 % of the data, while the remaining 20 % is the test set. The function of the training set is to develop a prediction model, while the task of the testing dataset is to validate it. Next, random extraction of the model hyperparameters is performed using the training set. Then, grid-search method is performed to obtain the optimized result [48]. k-fold cross validation scheme is used to further enhance the training models' accuracy. This study selects 10-fold cross-validation, resulting in the training dataset being divided into 10 equal subsets. Out of these, one subset is considered for validation and the remaining nine subsets is used for model training. This selection process of training and validation sets is repeated 10 times till each subset is considered for cross-validation [49]. SHapley Additive exPlanations (SHAP) [50] is a mathematical method that is used to explain the predictions of ML models. It is based on the concept of game theory and can explain the contribution of each feature to the prediction. After selecting the best performing model, SHAP is used to provide a better understanding of the relation between input and output features. A flow chart representing the ML model workflow is presented in Fig. 2. Data normalization is often performed in ML studies for improving the model performance, which converts the range of values in numerical features. Normalization can be useful for linear models and interpreting their coefficients as variable importance. However, this study employed SHAP for model interpretation and understanding the input-output relationship. Although many studies have utilized different data normalization techniques, some recent studies [35,36] showed that ML models can perform reliably without adopting any data normalization technique.

Different performance metrics are evaluated in this study to determine the performance of data-driven ML models. The parameters used to indicate the model's accuracy and precision are summarized in Table 2. Those parameters are the Coefficient of Determination (R^2), Root Mean Square Error (*RMSE*), Mean Absolute Error (*MAE)*, Nash Sutcliffe Efficiency (*NSE*) and Index of Agreement (*d*). R^2, *NSE* and *d* determines the model accuracy, while *RMSE* and *MAE* are error quantification parameters.

4. Discussion of ML model results

4.1. Interpretation with standard metrices

As discussed in the previous section, R^2, *RMSE*, *MAE, NSE* and *d* are the five important metrics for determining the model accuracy. The performance measures obtained from this study are summarized along with the 10-fold cross validations results in Table 3 and Table 4. From Table 3, it can be observed that for circular cross sections, XGB and CatB exhibit the least error with *MAE* values of 56.02 and 51.09, respectively in the training set, while the same for test set are 91.22 and103.05. *SVR* gives the highest error value of 435.85 and 465.15 in the training and testing set, respectively. A similar trend is seen while evaluating the *RMSE* error. It is observed in the testing phase that XGB and CatB gives high R^2 values of 0.976 and 0.967 while in training the values are 0.995 and 0.996, respectively. SVR predicts R^2 value of 0.531 and 0.647 for training and testing, respectively. The *NSE* and *d* values for CatB model are 0.985 and 0.989, respectively. For rectangular columns (Table 4), XGB and CatB also provide the least error values of 99.80 and 93.13, respectively for testing. These two algorithms achieved the highest accuracy with R^2 values of 0.991 and 0.993, respectively along with *NSE* and *d* values of 0.994 and 0.999 for CatB. Since, the CatB model has the least error values and the highest R^2 amongst the other models for both

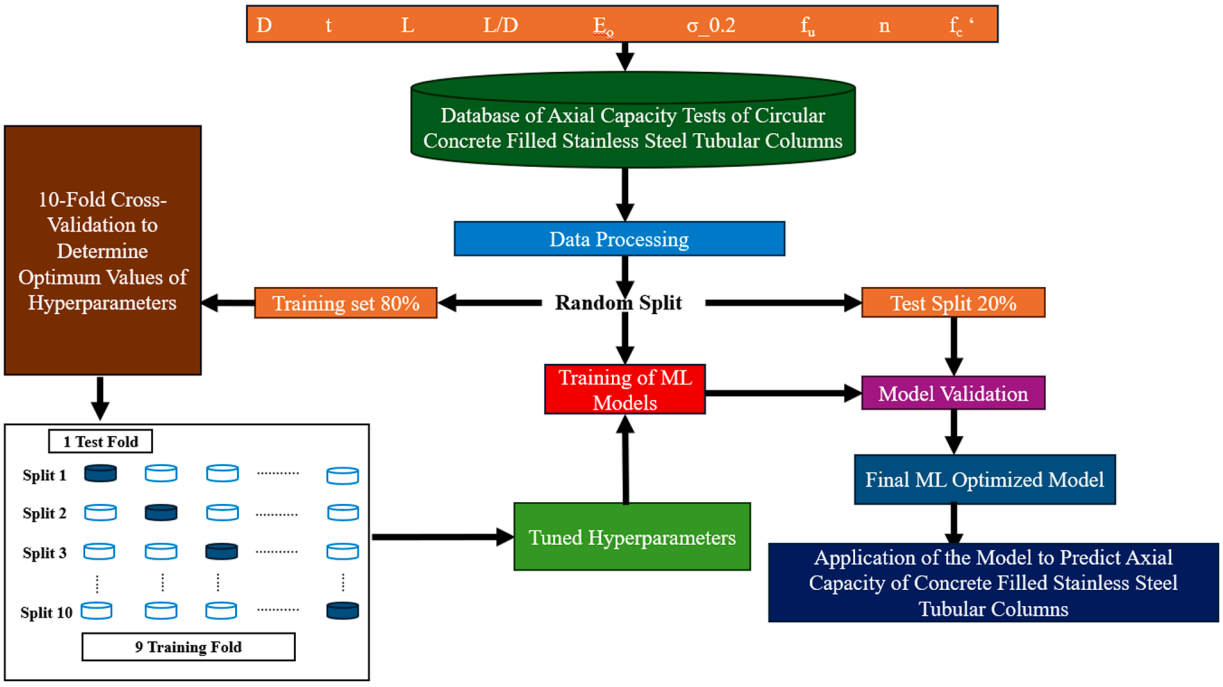

Fig. 2. Machine Learning workflow.

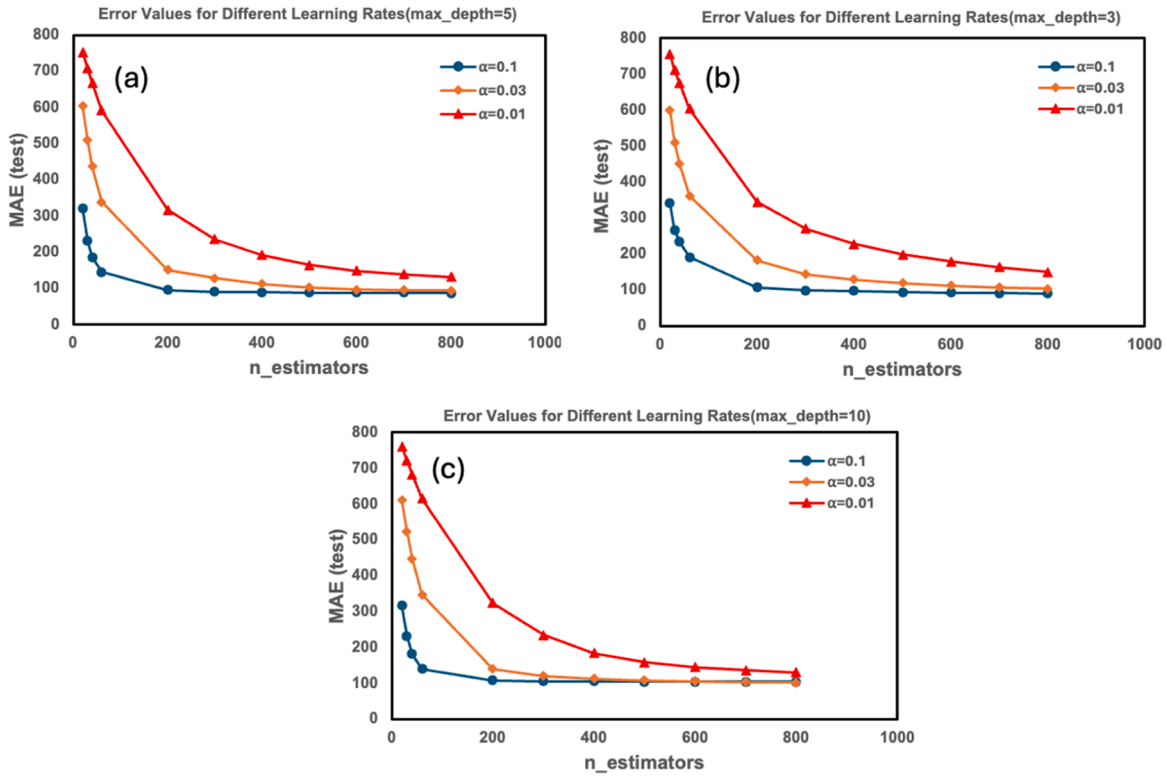

Fig. 3. Hyperparameter tunning of CatB for circular columns using different max depth.

type of cross-sections, it can be regarded as the best ML model. The most important factor behind success of XGB and CatB models is their scalability in different scenarios. XGB is an advanced ensemble learning model that combines different base learners for better performance. In CatB, the decision trees are built iteratively which leads to further increase in model performance. Both algorithms have enhanced loss function and optimization process as well as a regularization parameter to overcome overfitting. Furthermore, the CatB has the R^2, *NSE* and *d* values closest to 1 as compared to other algorithms and subsequently CatB is selected for further analysis.

4.2. *Improvement of model efficiency with hyper-parameter tuning*

Hyperparameter tuning is important for improving algorithm

Table 2
Formulas to determine accuracy of Machine Learning models.

Performance Metrics	Notation	Formula
Coefficient of Determination	R^2	$R^2 = 1\text{-}\frac{\sum_{i=1}^{m}(P_i - A_i)^2}{\sum_{i=1}^{m}(P_i - \overline{A})^2}$
Root Mean Square Error	*RMSE*	$RMSE = \frac{\sqrt{\sum_{i=1}^{m}(P_i - A_i)^2}}{m}$
Mean Absolute Error	*MAE*	$MAE = \frac{\sum_{i=1}^{m}\lvert(P_i - A_i)\rvert}{m}$
Nash Sutcliffe Efficiency	*NSE*	$NSE = 1\text{-}\frac{\sum_{i=1}^{m}(P_i - A_i)^2}{\sum_{i=1}^{m}(A_i - \overline{A})^2}$
Index of Agreement	*d*	$d = 1\text{-}\frac{\sum_{i=1}^{m}(P_i - A_i)^2}{\sum_{i=1}^{m}(\lvert Pi - \overline{A}\rvert + \lvert Ai - \overline{A}\rvert)^2}$

performance and obtaining optimized results. The grid search method [38] is used to obtain the values of the hyperparameters. A detailed description of hyper-parameters used in ML models are provided in Table 5. For the CatB model, three parameters, such as the number of trees (n_estimators), depth of the tree (max_depth), and learning rate (α) have the highest influence on the model performance and hence discussed in detail. The effect of these parameters on model performance are studied and presented in Fig. 5. It is evident that the smallest absolute error is linked with max_depth= 3, n_estimators= 800, and α= 0.1. Since, the hyperparameter tuning technique is similar for both types of columns, only one set of graphical representation is sufficient to provide an overview of the entire process.

4.3. Interpretation of CatBoost model using SHAP values

The Global Interpretability feature of the SHAP modeling system ranks each input parameter based on their importance and signifies the positive and negative correlation with the output. The features are represented on y-axis with the highest impactful feature at the top and the least one at the bottom. Along the horizontal axis, specific point color depicts which feature impacts the output positively (red) or negatively (blue). SHAP plots for both types of cross sections are shown in Fig. 4. Interestingly, both the plots reveal that the tube thickness (t) is the most significant parameter in governing the axial capacity of CFSST columns. As discussed before, thickness is a crucial factor in predicting axial capacity of regular CFST columns. Similarly, *D, H, B, L* are also important factors [34–36]. But in CFSST columns, the grade of SS is also crucial which is in accordance with results obtained from various literatures. Tao et al. [7] compared the axial capacities of four different grades of SS which included one ferric (EN1.4003), two austenitic (EN 1.4301 and 1.4401) and one duplex (EN1.4462). It was found that when the steel grade changed from ferric to austenitic, axial strength increased by 1.5 %. The proof stress ($\sigma_{-0.2}$) of SS also has a significant effect on the axial capacity of CFSST columns [5]. This can be further justified from the SHAP plots as proof stress is ranked higher than the ultimate stress (f_u) for both circular and rectangular sections. Since, the red dots are on the right side of the horizontal (x) axis and blue dots on the left side, this signifies that the grade of SS and proof stress has a positive correlation with the axial capacity.

The local interpretability for both sections is explained using waterfall plots [51] in Fig. 5 where the expectation value ($E[f(x)]$) depicts the dataset mean value and the output ($f(x)$) is the final prediction by the CatB model. *D, H, B, L* and *t* have high SHAP values amongst other features which gives further evidence of their importance in predicting axial capacity. A waterfall plot depicts the contribution of every parameter in deviating the value from the mean for a particular input data. For circular columns, the mean predicted axial capacity value is 1766 kN whereas the result generated by the CatB model is 1699 kN. The experimental result for given design data is 1707 kN. Similarly, for rectangular cross sections, the mean is 1570.7 kN and the predicted value is 1892.4 kN. The observed experimental value for the particular column is 1947 kN.

5. Comparison with design code equations

In order to further assess the accuracy and acceptability of the CatBoost model, the results are compared with different design code

Table 3
Performance measure for circular CFSST columns.

Training Set					Testing Set				10-fold CV
Model	***RMSE***	R^2	**Adjusted R^2**	***MAE***	***RMSE***	R^2	**Adjusted R^2**	***MAE***	**Mean R^2**
LR	270.607	0.940	0.936	207.527	251.855	0.943	0.923	206.989	0.919
RR	278.726	0.937	0.932	208.638	247.725	0.945	0.925	205.589	0.917
Lasso	270.607	0.940	0.936	207.527	251.854	0.943	0.923	206.988	0.919
KNN	36.241	0.999	0.999	9.773	173.501	0.973	0.963	110.947	0.907
SVR	758.401	0.531	0.497	435.852	627.23	0.647	0.521	465.151	0.503
DT	125.626	0.990	0.990	119.773	291.188	0.924	0.897	143.167	0.892
RF	494.923	0.800	0.786	139.624	274.443	0.932	0.908	152.965	0.806
XGB	74.457	0.995	0.995	56.023	139.520	0.973	0.976	91.228	0.962
AdaB	265.519	0.942	0.938	222.538	337.260	0.898	0.862	297.228	0.858
CatB	**68.204**	**0.996**	**0.996**	**51.091**	**165.416**	**0.975**	**0.967**	**103.053**	**0.958**

Table 4
Performance measure for rectangular CFSST columns.

Training Set					Testing Set				10-fold CV
Model	***RMSE***	R^2	**Adjusted R^2**	***MAE***	***RMSE***	R^2	**Adjusted R^2**	***MAE***	**Mean R^2**
LR	700.777	0.918	0.912	545.29	669.338	0.859	0.815	553.501	0.826
RR	702.708	0.917	0.912	539.60	664.087	0.861	0.818	548.274	0.833
Lasso	700.794	0.918	0.912	545.05	669.888	0.859	0.815	553.592	0.826
KNN	138.616	0.997	0.997	18.99	173.555	0.991	0.998	91.93	0.956
SVR	2268.29	0.136	0.081	858.45	1610.979	0.184	−0.070	460.82	0.187
DT	198.024	0.995	0.995	118.23	177.591	0.990	0.977	190.542	0.934
RF	251.670	0.989	0.989	72.95	217.857	0.985	0.980	123.135	0.941
XGB	114.770	0.998	0.998	69.44	172.491	0.991	0.988	99.804	0.978
AdaB	246.650	0.990	0.989	186.85	298.898	0.972	0.963	252.59	0.954
CatB	**115.050**	**0.998**	**0.998**	**62.29**	**146.125**	**0.993**	**0.991**	**93.136**	**0.976**

Table 5
List of hyperparameters for the proposed ML models.

Model	Hyperparameters	Value
LR	a. Normalization	True
RR	a. Learning Rate	1
	b. Random State	80
	c. Normalization	False
	d. Fit Intercept	bool
Lasso	a. L a. Learning Rate	0.0001
KNN	a. Number of neighbors	7
	b. Weights	distance
SVR	a. C	5
	b. Degree	1
DT	a. Random State	5000
RF	a. Random State	2
	b. Number of Estimators	1
XGB	a. Number of Estimators	100
	b. Learning Rate	0.1
	c. Gamma	0
	d. Subsample	0.75
	e. Max_depth	3
AdaB	a. Random State	30
	b. Number of Estimators	50
CatB	a. Number of Estimators	800
	b. Learning Rate	0.01
	c. Max_depth	3
	d. Metric_period	75

equations. The six provisions used in this study are GB 50936 [21], AISC 360–16 [11], EC 4 [13], AIJ-2008 [52], AS/NZS 2327 [19] and CSA S16–19 [53]. A detailed explanation of the codes is provided in Appendix A. Since, there is no specific code for SS, the equations for the conventional CFST columns are used. As mentioned previously, the code equations don't yield very accurate results. One of the primary reasons is due to the restricted values of different inputs such as concrete strength and steel strength. For example, in GB 50936 and EC4, high strength materials have not been included. Also, the steel yield strength (f_y) is up to only 460 MPa [54]. Material limits for the different code equations are given in Table 6 where f_{cu} is the cube strength and f_c' is cylinder strength.

Table 6
Material strength limits for CFST column in different design standards.

Design Codes	Concrete Strength (MPa)	Steel Strength (MPa)
GB 50936	$30 \leq f_{cu} \leq 80$	$235 \leq f_y \leq 460$
AISC 360–16	$21 \leq f_c' \leq 69$	$f_y \leq 525$
EC4	$20 \leq f_c' \leq 60$	$235 \leq f_y \leq 460$
AIJ−2008	$18 \leq f_c' \leq 90$	$f_y \leq 800$
AS/NZS 2327	$20 \leq f_c' \leq 120$	$f_y \leq 690$
CSA S16–19	$20 \leq f_c' \leq 80$	$f_y \leq 690$

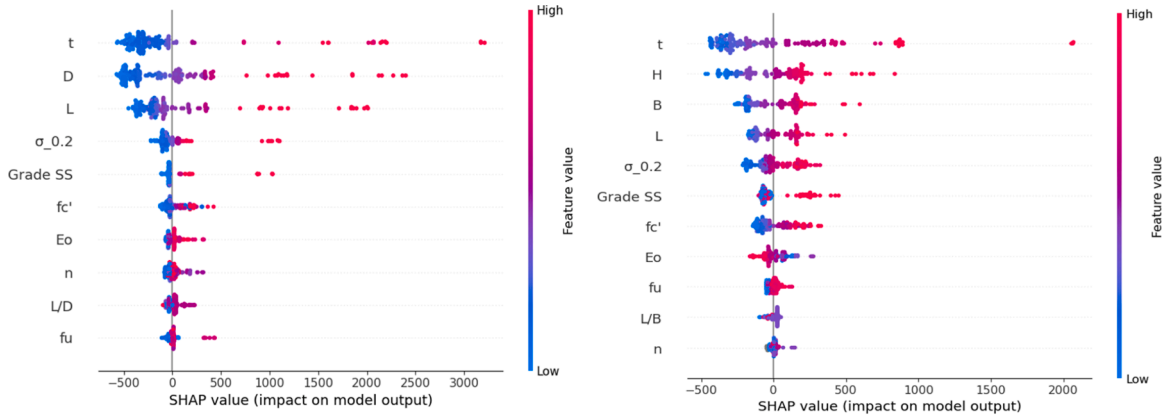

(a) (b)

Fig. 4. SHAP summary for **(a)** circular and **(b)** rectangular CFSST columns.

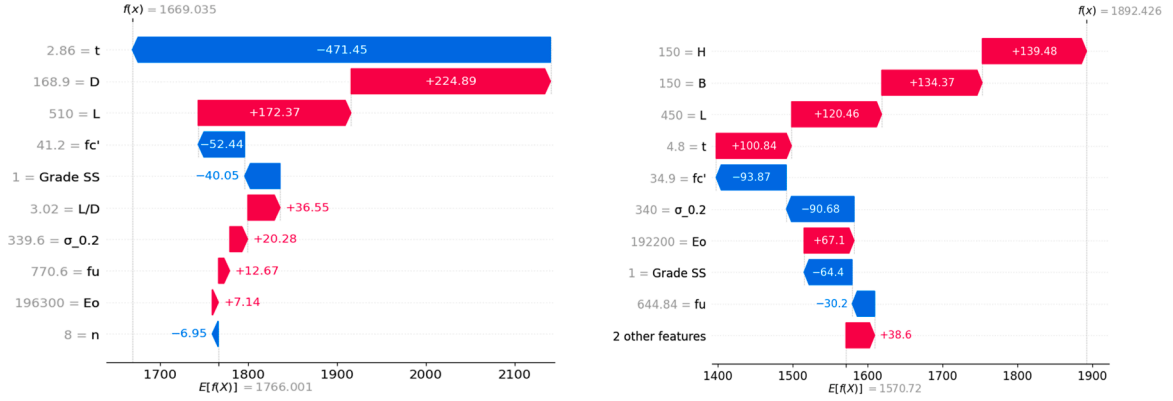

(a) (b)

Fig. 5. Waterfall plots for **(a)** circular and **(b)** rectangular CFSST columns.

5.1. Interpretation of model and code equation results using standard metrics

Standard metrics such as *MAE*, *RMSE, NSE* and *d* indicate model accuracy and are used to compare the results from ML model and the code equations. Mean Absolute Error (*MAE*) is the average of the errors between observed and predicted values. Root Mean Squared Error (*RMSE*) is the square root of the average between observed and predicted values. Nash Sutcliffe Efficiency (*NSE*) refers to a normalized statistic that determines the relative magnitude of residual variance to that of the normalized variance. NSE values range from negative infinity to 1, with 1 indicating a perfect match between simulated and observed values. The Index of Agreement (*d*) is a statistical measure used to evaluate the accuracy of model predictions by comparing them to observed data. It ranges between 0 and 1. A value of 1 indicates a perfect match between predicted and observed data, while 0 suggests no agreement at all [31]. A summary of error values is given in Tables 7 and 8 for circular and rectangular CFST columns, respectively. It is noted that for circular columns, CatB provides the minimum *MAE* and *RMSE* values of 113.8 and 11.8, respectively and therefore is the best performing ML model. The *NSE* and *d* values are 0.985 and 0.989, respectively. The second-best fit is AIJ-2008 with *MAE* value of 195.11 and *RMSE* value being 25.39. Similarly, for rectangular columns, CatB turns out to be the most accurate model with *MAE* value of 68.04 and *RMSE* value of 7.13. CSA S16–19 came out as the second most accurate model with *MAE* and *RMSE* of 177.97 and 19.68 along with *NSE* and *d* values of 0.994 and 0.999, respectively. A graphical representation is provided in Figs. 6 and 7.

5.2. Verification of model and design codes using error distribution and 1:1 diagonal line

An interesting way to compare the accuracy of the different models is to calculate the error distributions. Error percentages of the models are calculated and then divided into seven groups. Fig. 8 represents error ranges and their corresponding number of samples for both types of cross-sections. It can be inferred that the models with the maximum number of samples in the ranges of (0−5) % and (5−10) % are the most accurate. It is observed for circular columns, CatB has 92 and 39 samples and AIJ-2008 has 50 samples and 63 samples in the above-mentioned ranges. Hence, it can be concluded that CatB is the best performing model for predicting CFSST axial capacity. Equation prescribed in AIJ-2008 provided the best result amongst all different codes. In case of rectangular columns, it was observed that CatB has 131 and 44 samples and CSA S16–19 has 63 and 49 samples in the error ranges of (0−5) % and (5−10) %, respectively. CatB and CSA S16–19 provide the most accurate predictions for rectangular CFSST columns. Both sets of observations are in accordance with the results obtained from comparison with standard metrics in the previous section.

Another interesting procedure to evaluate prediction efficiency is to plot the experimental axial capacity against the predicted capacity by design codes and CatB model with a 45° line to classify the conservative/un-conservative characteristics of the code equations and ML model (Fig. 9). The less scattered the points are from the line, the more accurate is the prediction. Points below the line depicts that the predictions are conservative whereas the unconservative predictions are presented by points above the 45^0 line.

Table 7
Model performance measures for circular CFSST columns.

Models	*MAE*	*RMSE*	*NSE*	*d*
GB 50936	383.76	55.81	0.587	0.621
AISC 360–16	361.76	50.81	0.603	0.699
EC4	356.35	53.24	0.622	0.711
AIJ−2008	195.11	25.39	0.807	0.892
AS-ZNS 2327	356.35	53.24	0.622	0.711
CSA S16–19	465.90	53.58	0.211	0.321
CatB	**113.83**	**11.80**	**0.985**	**0.989**

Table 8
Model performance measures for rectangular CFSST columns.

Models	*MAE*	*RMSE*	*NSE*	*d*
GB 50936	512.08	58.26	0.192	0.265
AISC 360–16	221.88	26.29	0.791	0.882
EC4	512.09	58.26	0.192	0.265
AIJ−2008	322.47	35.49	0.643	0.721
AS-ZNS 2327	221.17	27.56	0.793	0.823
CSA S16–19	177.97	19.68	0.921	0.981
CatB	**68.04**	**7.13**	**0.994**	**0.999**

It is justified that the three design codes (AISC 360–16, GB 50936 and EC4) underestimates the axial capacity as most observations are below the 45° line. This confirms the conclusion drawn by Dai et al. [20] where they found that EC4 [13] yielded over-conservative results for circular CFSST columns. Similarly, other three design codes AS/NZS 2327 [19], AIJ-2008 [52], CSA S16–19 [53] yielded unconservative results. When the CatB model is compared, it is seen that the predicted values are closer to the 45^0 line. This indicates that the CatB model has outperformed all code prescribed equations in accurately calculating the CFSST columns axial capacity.

It is observed from Fig. 10 that the axial capacity of rectangular CFSST columns calculated by the different code equations are lower than the experimental ones as majority of the points lie below the 45° line. This means the axial capacity of the rectangular columns are overestimated by design codes as was the case for circular ones. However, for the CatB model, the points lie along the 45° diagonal line with minor deviations. This findings are consistent with the results obtained by Yan et al. [55] where compressive strength of CFFSST short columns were investigated using Finite Element (FE) modeling. In a study by Liao et al. [56], 48 circular and square CFSST columns were experimentally tested under axial compression. The test results were compared with different code equations and EC4 [13] found to underpredict the experimental results. Another interesting observation from Figs. 9 and 10 is that the accuracy of the experimental data and the ones predicted by different codes decreases when the capacities are beyond 2000 kN. The mean R^2 value obtained for results below 2000 kN is approximately 98.76 whereas the mean value decreases to 91.5 for results above 2000 kN for both circular and rectangular columns. This can be attributed to the fact that code equations were developed based on certain ranges of geometric and material properties and not enough experimental results are present to cover all ranges of values. Most of the experiments were also for small scale specimens with smaller cross section size. The grade of SS has an important role to play in increasing the axial capacity of CFSST columns [7]. Since the code equations used for comparison are developed for CFST columns, the effect due to SS grade is not considered and this can be regarded as one of the primary limitations of the available code equations. Cakiroglu et al. [35] utilized different ML models to predict the axial compressive capacity of CFST columns. The experimental results were compared with code equations, and it was inferred that the accuracy varied for different ranges of input parameters. For instance, the yield strength of steel (f_y) between 0 and 200 MPa resulted in the R^2 value of 0.766. When the range of f_y was between 200 and 400 MPa the R^2 value increased to 0.887 for AISC 360–16 [11]. A change in the range of compressive strength of concrete (f_c') from 25 to 50 MPa to 50–100 MPa resulted in a decrease in prediction accuracy from 0.941 to 0.930 for EC4 [13]. However, the CatB model developed in this study counteracts this deviation in CFSST column's axial strength prediction and provides accurate results with R^2 value of 0.9956 irrespective of the lower or higher axial strength observed in experimental studies.

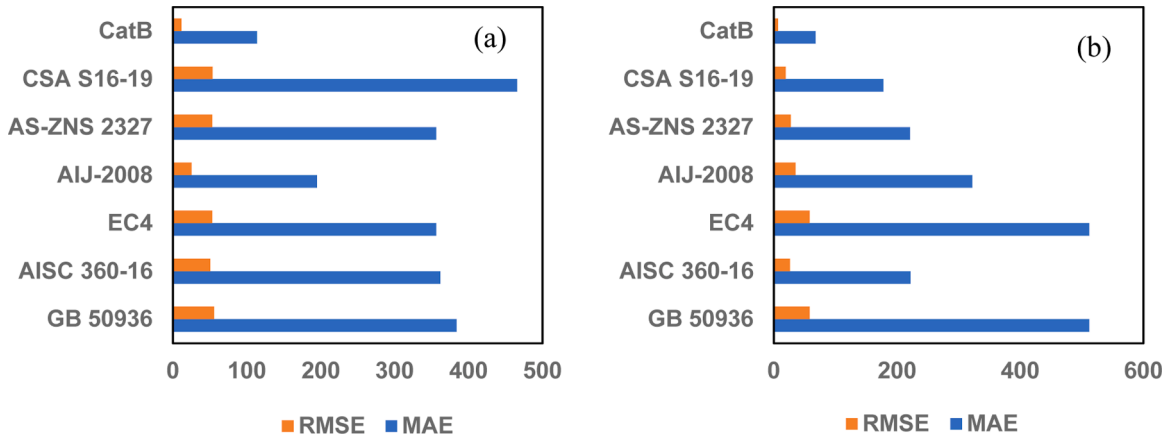

Fig. 6. Comparison between existing codes and CatB model with respect to *MAE* and *RMSE* for **(a)** circular and **(b)** rectangular CFSST columns.

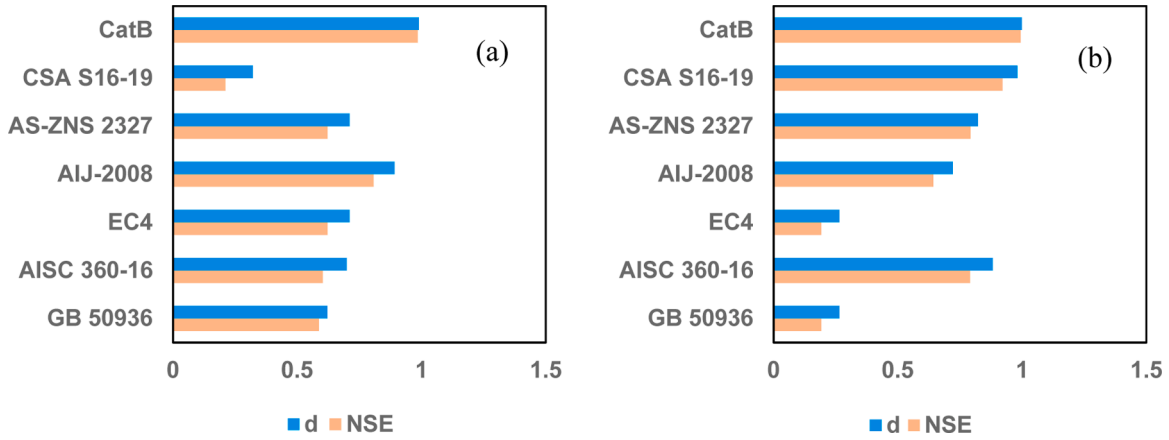

Fig. 7. Comparison between existing codes and CatB model with respect to *NSE* and *d* for **(a)** circular and **(b)** rectangular CFSST columns.

5.3. *Comparison of model performance using Taylor diagram*

Taylor diagrams representing the relationship between the standard deviation (*SD*) and Pearson correlation coefficient (*R*) of the predicted axial capacity is shown in Fig. 11. The *SD* of experimental data for circular and rectangular columns are 2336.052 kN and 1099.145 kN, respectively and is the reference point. CatB has the highest *R* of 0.9986 for circular and 0.9971 for rectangular CFSST columns. It is observed that CatB also has the *SD* of 2280.9 kN and 1081.7 kN and is the nearest to the experimental outcomes. AIJ-2008 [52] has the *SD* of 2057.02 kN and correlation coefficient of 0.9921 which made it the second best model for circular CFSST columns. For rectangular ones, AIJ-2008 [49] is the second most accurate model with R value of 0.9975 and standard deviation of 991.25 kN

6. Reliability analysis

Though the CatB model estimates CFSST columns' axial capacity with notable precision, it is essential to check if this model abides by the reliability aspects of design specifications. Uncertainties in the design process is taken into consideration using the resistance factor (φ) in load and resistance factor design (LRFD). The resistance factor is inversely related to a reliability index (β) which signifies the probability of failure. The likelihood of failure decreases with increasing reliability index. Eq. (1) establishes a relation between the nominal resistance and load demand of a structure in limit state where R_n represents the nominal resistance, Q_i is loading demand and γ_i is load safety factor [31].

$$\varphi R_n \geq \sum \gamma_i Q_i \tag{1}$$

Eq. (2) obtained from studies by Cakiroglu et al. [35] and Sener and Varma [57] is used to calculate the resistance factor (φ).

$$\varphi = P * M * F * e^{(-\alpha\beta V)_R} \tag{2}$$

In Eq. (2), P is obtained by taking the mean of the ratios of experimental values ($N_{\_measured}$) and the corresponding values predicted by the CatB model ($N_{\_predicted}$) for all samples in the dataset for circular and rectangular CFSST columns. For circular and rectangular cross sections, the values of P are 0.9625 and 0.90, respectively. F is the ratio of measured to nominal cross-section properties and is assigned a value of 1.0 [35]. The value of the average ratio of mean to measured nominal material strengths, M is considered to be 1.19 based on the recommendation by Thai et al. [58]. The reliability index and the linearization approximation constant are represented by β and α, respectively. Furthermore, Eq. (3) is used to calculate the coefficient of variation of resistance (V_R) where V_m, V_f and V_p denote the coefficient of variations of material properties, fabrications and ($N_{\_predicted}/N_{\_measured}$) ratio.

$$V_R = \sqrt{V_m^2 + V_f^2 + V_p^2} \tag{3}$$

The V_m and V_f are considered as 0.193 and 0.05 based on studies by Sener and Verma [57] and Galambos [59], respectively. The values of V_p are calculated as 0.1614 and 0.0824 for circular and rectangular columns, respectively and subsequently, V_R is calculated as 0.2565 and 0.2157. As suggested by Galambos [59] and Sener and Varma [57], β and α are assumed to be 3.0 and 0.55, respectively. Using all these values in Eq. 2, a resistance factor of 0.75 is obtained for both type of cross sections which is equal to the resistance factor prescribed by AISC

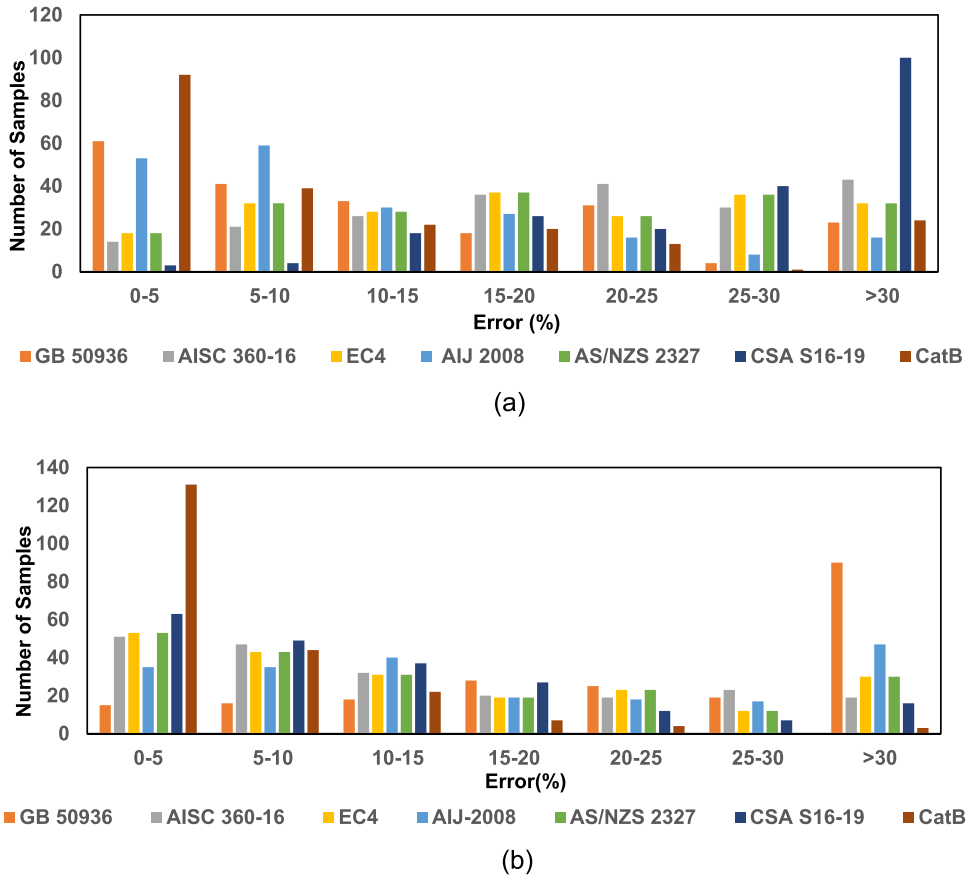

Fig. 8. Bar chart representing error ranges for (a) circular and (b) rectangular CFSST columns.

360–16 [11]. Hence, it is verified that the developed CatB model is structurally reliable and can be used to predict the axial capacity of CFSST columns.

7. Graphical User Interface (GUI)

A Graphic User Interface (GUI) is developed with Python programming language and Streamlit framework (https://streamlit.io/) to enable prompt and convenient prediction of axial capacity of CFSST columns by the CatB model. Snapshot of the developed GUI is shown in Fig. 12 for rectangular CFSST columns. In the left side, there is a tab for selecting the type of cross section for axial capacity prediction. On the right side, there are input parameters which the user can adjust. The final predicted axial capacity for the particular input data can be found at the bottom of the GUI. Cross-section diagram is also added to the interface to provide a better understanding of the input features. Although the developed GUI can be used for predicting the axial capacity of CFSST columns, the develop ML model is limited by the following conditions:

$50 \leq B \leq 250$ (mm); $1.8 \leq t \leq 12.8$ (mm); $50 \leq H \leq 250$ (mm); $150 \leq L \leq 700$ (mm); $1.5 \leq L/B \leq 6.0$; $2.49 \leq L/D \leq 6.02$; $400 \leq f_u \leq 830$ (MPa); $170 \leq E_0 \leq 210$ (GPa); $20 \leq f'_c \leq 150$ (MPa); and $1.8 \leq n \leq 8.2$. The GUI is free to access and the related dataset are provided on GitHub (https://cfsst-columns.streamlit.app/).

8. Limitations and future research directions

Although the developed ML model can provide accurate prediction results, there are some limitations. This study only considered concentrically loaded columns and limited to short columns. The effect of residual stresses, imperfections and confinement were not considered while developing the ML models. Also, due to the different modelling assumptions such as mesh size, element selection and boundary conditions in numerical analyses, some disparity in modelling may occur which can ultimately affect the dataset and hence ML model prediction. Keeping these limitations in mind, there is a need for further studies and development of more robust models for more accurate axial capacity prediction. Research should be conducted to develop experimentally validated numerical models considering wider parameter range to expand the current dataset. Large cross-sectional sizes and slender columns should also be used to enhance current database for ML-based axial capacity prediction. New research should also focus on predicting the failure modes of CFSST columns as limited research is conducted in this domain.

9. Concluding remarks

This study presents an explainable and efficient machine learning model to predict the axial capacity of the CFSST columns. This study comprises experimental and numerical datasets obtained through an extensive literature survey. The effect of the input parameters on the axial capacity is discussed. Ten ML models are compared to determine the best performing model. SHapley Additive exPlanations is implemented to find out how each input feature governs the output. The best performing ML model is compared with six design codes (GB 50936 [21], AISC 360–16 [11], EC4 [13], AIJ-2008 [52], AS-NZS 2327 [19] and CSA S16–19 [53]). Based on this study, the following conclusions are drawn:

- From the parametric analysis, it is observed that thickness *(t)* and column diameter *(D)* are the important parameters in predicting the axial load carrying capacity of circular CFSST columns. Similarly, for

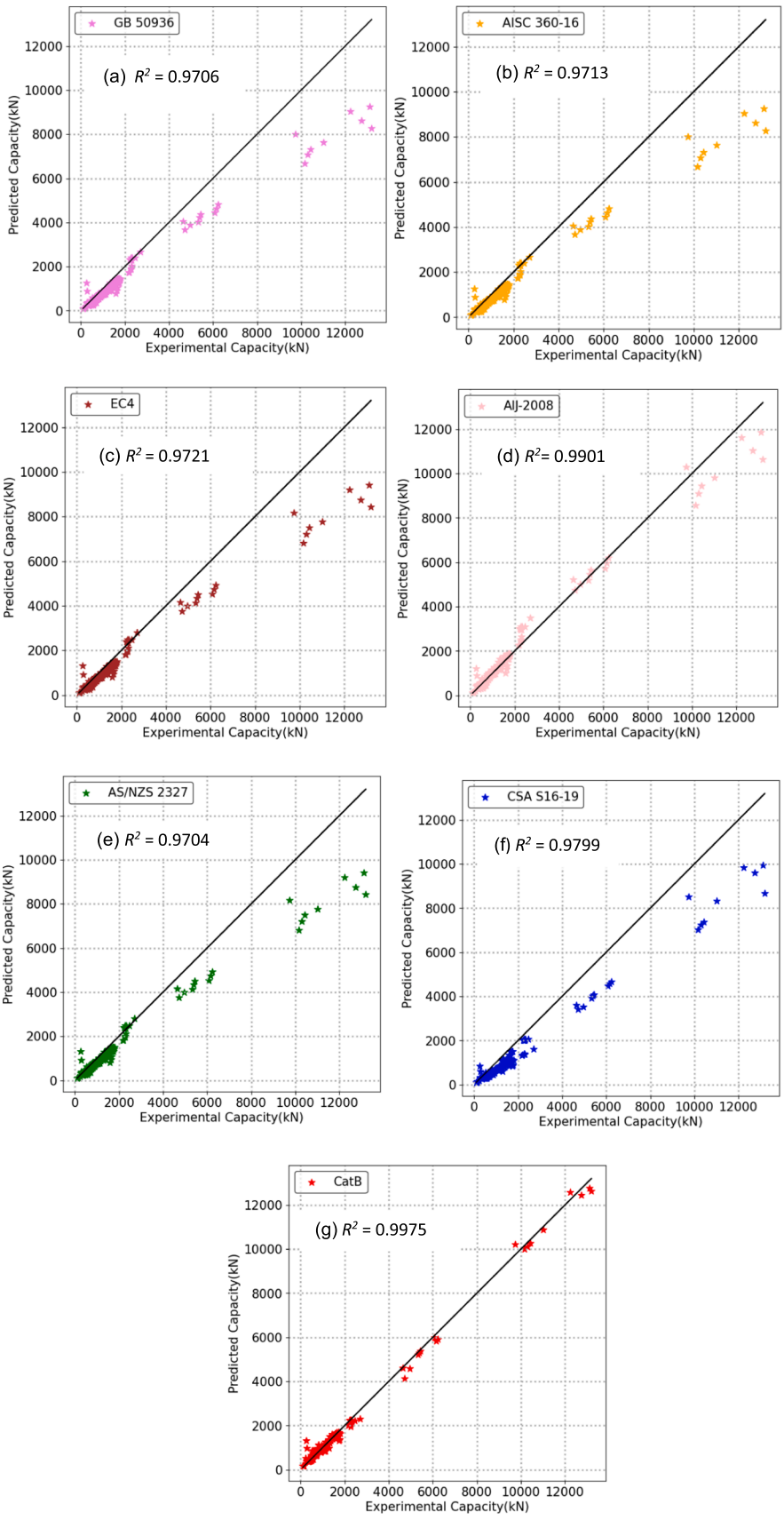

Fig. 9. Comparison between experimental and predicted axial capacity for circular CFSST columns by code equations and CatB model predictions.

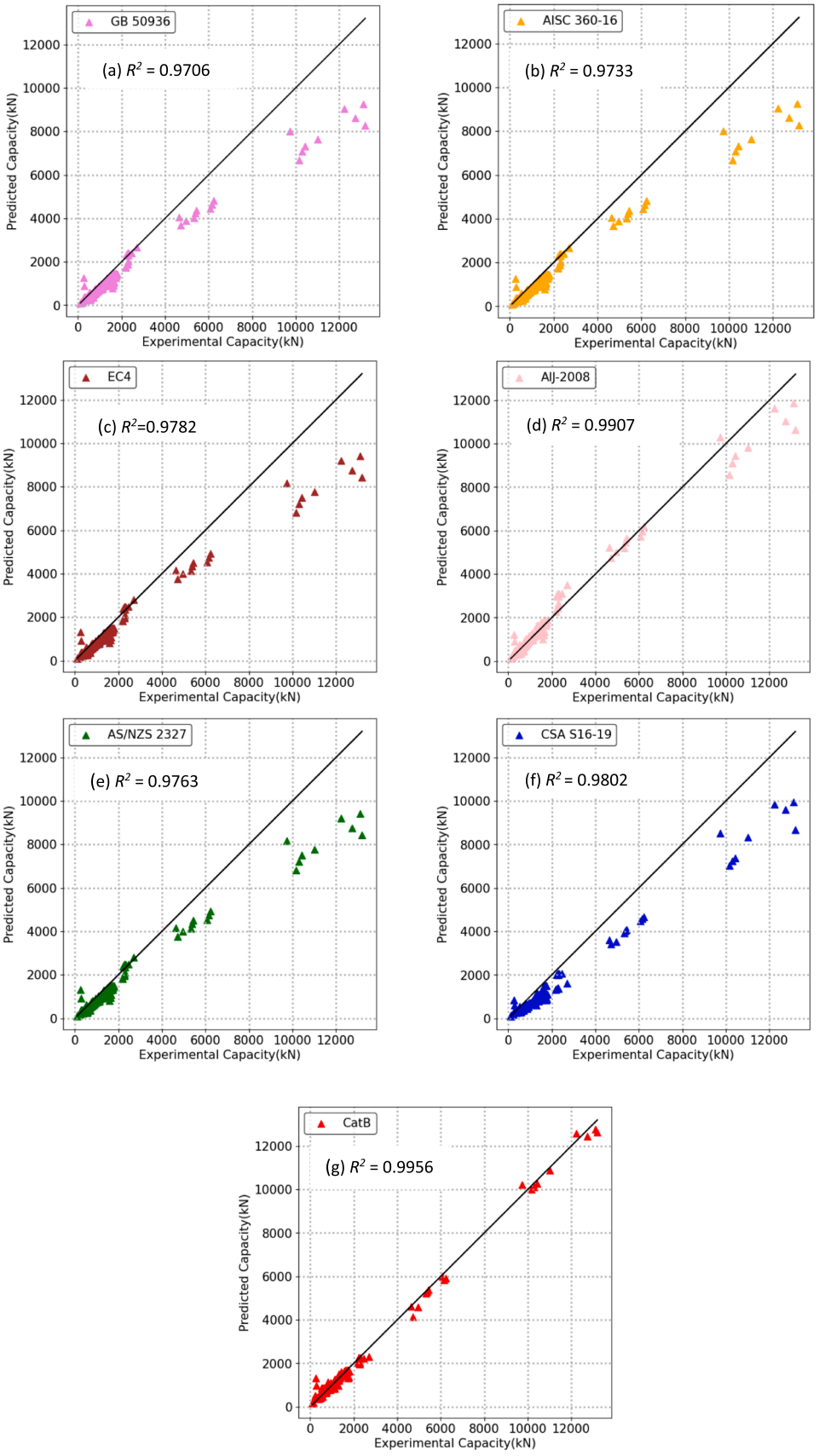

Fig. 10. Comparison between experimental and predicted axial capacity for rectangular CFSST columns by code equations and CatB model predictions.

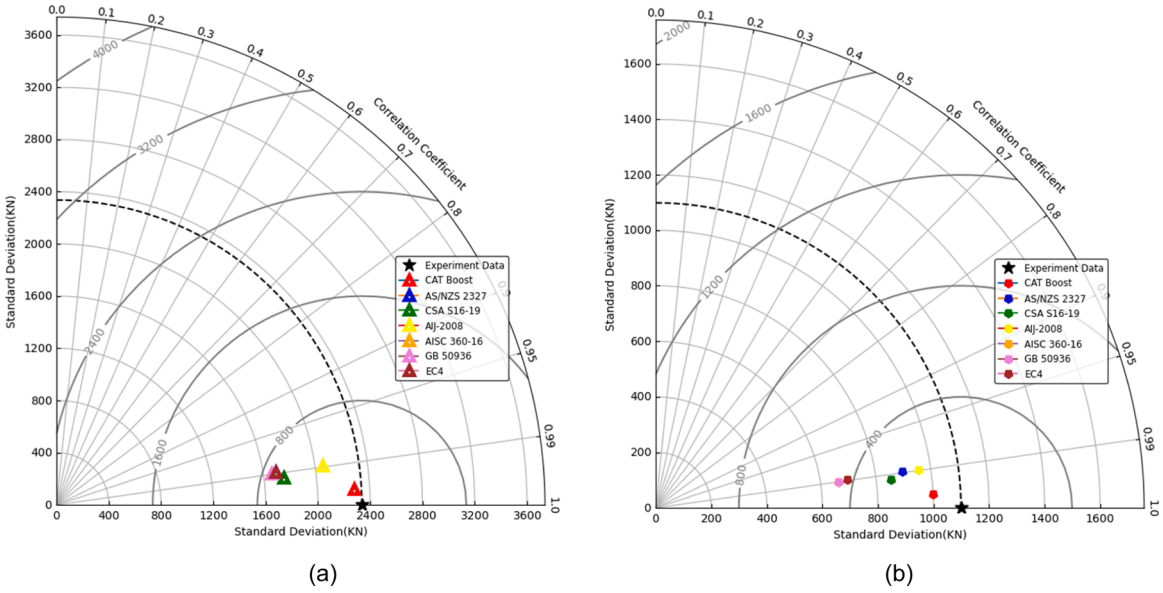

Fig. 11. Taylor Plots for (a) circular and (b) rectangular CFSST columns.

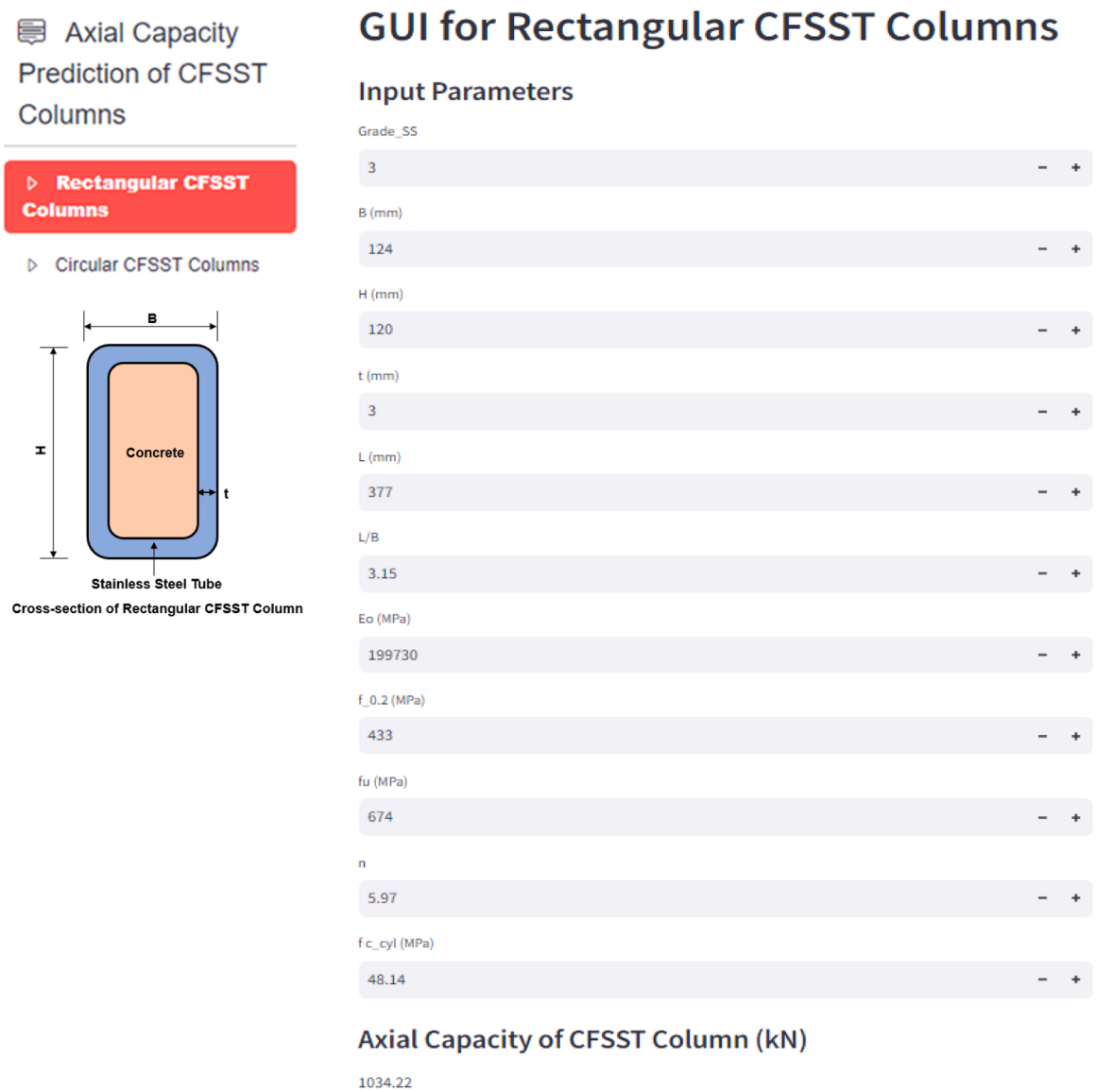

Fig. 12. GUI for CFFST columns.

rectangular ones, thickness (*t*), width (*B*) and height (*H*) are the most significant features. The grade of the stainless steel (*Grade_SS*) also considerably affects the axial capacity.

- The proposed CatB model is the most accurate ensemble learning model compared to the other ML models in terms of accuracy. CatB achieved a mean coefficient of determination value of 0.9975, MAE of 113.8 and RMSE of 11.80 for circular columns. For rectangular cross sections, CatB has R^2 value of 0.9956, MAE of 68.04 and RMSE of 7.13.
- From SHAP, it is revealed that thickness (*t*), diameter of circular columns (*D*) and height of rectangular columns (*H*) are the most important parameters affecting the axial capacity. The greater the thickness, more is the capacity which is also true for CFST columns. But one significant difference, is that SS grade plays a pivotal role for CFSST columns which is not likely the case for the CFST columns. Also, *Grade_SS* has a positive correlation with strength.
- Amongst the different design codes, AIJ-2008 has the least *MAE* and *RMSE* for circular and rectangular CFSST columns. Upon performing error analysis of the design codes and model with experimental data, it is obtained that CatB has the maximum number of values in the error range of (0−5) % which is followed by AIJ-2008 for circular columns. For the rectangular ones, CSA S16–19 succeeds CatB in terms of maximum number of samples in the above-mentioned error range.
- From the 45° trend-line it can be concluded that the design codes yielded conservative results for circular and rectangular CFSST columns. The underestimated axial capacity of columns are in accordance with studies conducted by [51–53].
- A notable difference between experimental and code results are observed when the results are more than 2000 kN. The mean R^2 value obtained for results below the above limit is approximately 98.76 whereas the mean is 91.5 for results above 2000 kN for both circular and rectangular columns.
- Further justification for the efficiency of CatB model is explained through Taylor Plots. For both cross sections, CatB has the deviation value closest to the experimental standard deviation. The Pearson correlation coefficients are also the highest amongst other models (0.9986 for circular and 0.9971 for rectangular columns).
- The LRFD method's reliability analysis result demonstrates that with a reliability index of 3, the resistance factor comes out to be 0.75, per the guidelines provided by AISC 360–16.

Hence, it can be thoroughly justified that CatB model generated in this study considering the wide range of variation in material and geometric properties can be considered as the most accurate model for axial capacity prediction of CFSST columns. It is noted that for circular columns, although the codes can predict the axial capacity with noteworthy accuracy within a certain range of results, still the results are highly conservative. For the rectangular ones also, the code predicted axial capacities tend to be less than the experimental results though they have good correlation coefficients. This study does not denounce the existing design equations but tries to justify the need of a better model which can counteract the effect of design limitations and assumptions. The accuracy of the developed CatB model can help engineers design cost-efficient structures avoiding lengthy computations.

CRediT authorship contribution statement

Billah AHM Muntasir: Writing – review & editing, Resources, Project administration, Funding acquisition, Conceptualization. **Islam Kamrul:** Writing – review & editing, Methodology, Data curation. **Das Debarshi:** Writing – original draft, Visualization, Investigation, Data curation. **Roy Deeptarka:** Writing – original draft, Visualization, Validation, Software, Methodology, Formal analysis.

Declaration of Competing Interest

The authors declare that they have no known competing financial interests or personal relationships that could have appeared to influence the work reported in this paper.

Appendix A

Codes equations for calculating axial capacity of CFSST columns:
The calculation method of CFSST columns is shown as prescribed by different code eqautions.

1. **GB 50936 Provisions**

- $N_u^{GB} = f_{sc} \quad (A_s + A_c)$
- $f_{sc} = \left(1.12 + B\xi + C\xi^2\right) f_c$

where,
A_{ss} = *StiffenersArea*;
f_{ys} = Stiffeners Yield Strength
B and C = variables pertaining to steel yield strength f_y and concrete strength f_c.
N_u^{GB} = axial compressive strength of CFSST column.

2. **AISC 360–16 Provisions**

- $N_u^{AIS} = A_s f_c + 0.95 A_c f_c$
- $N_u^{AIS} = N_p - \left(N_p - N_y\right)\left(\frac{\lambda - \lambda_p}{\lambda_r - \lambda_p}\right)^2$
- $N_y = A_s f_y + 0.7 A_c f_c$

where,
λ = Section's slenderness ratio is equivalent to the proportion of diameter to thickness.
N_u^{AIS} = axial compressive strength of CFSST column.

3. **EC4 Provisions**

- $N_u^{EC} = \eta_s A_s f_y + A_c f_c \left(1 + \eta_c \frac{t}{D} \frac{f_y}{f_c}\right)$
- $\eta_s = 0.25(3 + 2\bar{\lambda}) \leq 1$
- $\eta_c = 4.9 - 18.5\bar{\lambda} + 17\bar{\lambda}^2 \geq 0$
- $\bar{\lambda} = \sqrt{\frac{N_{cr}}{A_s f_y + A_c f_c}}$
- $N_{cr} = \frac{\pi^2 (EI)_{eff}}{(L_e)^2}$
- $(EI)_{eff} = E_s I_s + 0.6 E_c I_c$

where,
$\bar{\lambda} = RelativeSlenderness; \bar{\lambda} \leq 0.5$
η_s and η_c = Coefficients of the CFST column which represents the confinement effect;
L_e = Effective length of the CFST column;
E_s = Elastic Modulus of the Exterior Steel tube;
E_{si} = Elastic Modulus of the Interior Steel tube;
E_{ss} = Elastic Modulus of Stiffeners;
I_s = Second Moments of Area of the Exterior Steel tube;
I_{si} = Second Moments of Area of the Interior Steel tube;
I_{ss} = Second Moments of Area of Stiffeners;
N_u^{EC} = axial compressive strength of CFSST column.

4. **AIJ-2008 Provisions**

- $N_u^{AIJ} = (1 + \phi_c) A_s f_c + A_c f_c$

where,
$\phi_c = Coefficient represents the simplified strength enhancement effect$;
N_u^{AIJ} = axial compressive strength of CFSST column.

5. **AS/NZS 2327 Provisions**

- $N_u^{As} = k_s \eta_s A_s f_y + A_c f_c \left(1 + \eta_c \frac{t}{D} \frac{f_y}{f_c}\right)$
- $k_f = \frac{\pi (D_e - t) t}{A_s}$
- $D_e = \min\left(\sqrt{\frac{\lambda_{ey}}{\lambda_p}}, \left(\frac{3\lambda_{ey}}{\lambda_p}\right)^2\right)$
- $\eta_s = 0.25(3 + 2\bar{\lambda}') \leq 1$
- $\eta_c = 4.9 - 18.5\bar{\lambda} + 17\bar{\lambda}^2 \geq 0$
- $\bar{\lambda}' = \sqrt{\frac{N_{cr}}{k_f A_s f_y + A_c f_c}}$
- $N_{cr} = \frac{\pi^2 (EI)_{eff}}{(L_e)^2}$
- $(EI)_{eff} = E_s I_s + E_c I_c$

where,
$\lambda_{ey} = limit of element slenderness$;
$\eta_s and \eta_c$ = Coefficients of the CFST column which represents the confinement effect;
N_u^{AS} = axial compressive strength of CFSST column.

6. **CSA S16–19 Provisions**

- $N_u^{Cs} = \frac{\tau \phi A_s f_y + \tau' \alpha_1 \phi_c A_c f_c}{\left(1 + \lambda^{2n}\right)^{1/n}}$
- $\tau = 1/\sqrt{1 + \rho + \rho^2}$
- $\tau' = 1 + \frac{25\rho^2 \pi}{D/t} \frac{f_y}{\alpha_1 f_c}$
- $\rho = 0.02(25 - D_0/L)$
- $\lambda = \sqrt{N_p/N_{cr}}$

- $\lambda = \sqrt{\frac{N_{cr}}{k_f A_s f_y + A_c f_c}}$
- $N_{cr} = \frac{\pi^2 (EI)_{eff}}{(L_e)^2}$
- $(EI)_{eff} = E_s I_s + \frac{0.6 E_c I_c}{1 + C_{fs}/C_f}$

where,
C_{fs} = Sustained Axial Load;
C_f = Total Load on the Column;
N_u^{Cs} = axial compressive strength of CFSST column.

Appendix B

Table B1
Database for Circular CFSST Columns

Reference	No of data	D (mm)	t (mm)	L (mm)	L/D	E_o (MPa)	$\sigma_{-0.2}$ (MPa)	f_u (MPa)	f_c (MPa)	n	Grade_SS
Uy et al. [5]	32	50.8–152.4	1.20–2.80	150–485	2.95-4.36	173900–195000	259–320	581.08–708	20–75.40	**7**-7.60	Austenitic/304
He et al. [8]	16	72.8–88.9	2.77–2.83	215–270	2.94–3.02	202000–206000	292–296	715–727	93.8–144.4	4.1–5.50	Austenitic/1.4301
Liao et al. [55]	24	159	2.88–4.50	480	3.02	177000–195000	383–401	647.69–691.32	33.76–46.96	3.13–7.07	Austenitic/304
He and Zhao [15]	18	72.80–89.30	2.79–3.13	214–265	2.93–2.98	201000–202000	258–321	673–729	49.60–63.60	3.80–4.90	Austenitic/1.4301
He et al. [20]	3	72.8–88.0	2.81–3.12	200–275	3.02	202000	286–301	567.20–963.10	92.8–140.0	3.30–4.30	Austenitic/1.4301
Lam and Gardner [16]	6	104–110	2.00–6.02	300	2.96–2.98	183600–202000	251–325	560–721	49.50–61.60	3.20–4.60	Austenitic/304
Yang [53]	**7**	50.2–150.6	2.86–7.9	211–400	2.36–2.91	183600–202000	251–325	560–721	49.50–61.60	3.20–4.60	Austenitic/304
Hou and Zhao [34]	17	50.8–130.80	1.80–6.3	215–403	2.06–2.93	183700–203000	255–320	532–734	49.50–62.80	3.00–4.50	Duplex/2205
Dai et al. [21]	37	51.3–78.60	2.80–7.83	200–275	2.36–2.91	183600–202000	251–325	560–721	49.50–61.60	3.20–4.60	Austenitic/316
Guo et al. [23]	22	50.6–200.6	2.86–7.9	211–400	2.36–2.91	175000–202000	230–321	564–723	49.50–61.40	3.80–4.30	Austenitic/1.4301
Li et al. [24]	29	48.2–155.6	2.81–7.93	203–404	2.31–2.95	183600–202000	251–325	500–761	49.00–61.70	3.30–5.20	Austenitic/304

Table B2
Database for Rectangular CFSST Columns

Reference	No of data	B (mm)	H (mm)	t (mm)	L (mm)	L/B	E_o (MPa)	$\sigma_{-0.2}$ (MPa)	f_u (MPa)	f_c (MPa)	n	Grade_SS
Uy et al. [5]	26	51–150	51–100.30	1.80–4.80	150–485	2.95-3.00	173900–195000	259–320	581.08–708	20–75.40	**7**-7.60	Austenitic/304
He et al. [8]	15	72.8–88.9	99.3–149.0	2.77–2.83	215–270	2.94–3.02	199000–217000	317–365	715–727	93.8–144.4	6.30–7.80	Chromium grade EN 1.4420
Liao et al. [55]	24	160	160	2.88–4.50	480	3.02	177000–195000	383–401	647.69–691.32	33.76–46.96	3.13–7.07	Austenitic/304
Young and Ellobody [18]	14	140.20–197.30	100–130	2.79–3.13	214–265	2.93–2.98	201000–202000	258–321	673–729	49.60–63.60	3.80–4.90	Duplex/1.4462
Azad et al. [60]	3	72.8–88.0	110–151	2.81–3.12	200–275	3.02	202000	286–301	567.20–963.10	92.8–140.0	3.30–4.30	Austenitic/1.4301

(continued on next page)

Table B2 (*continued*)

Reference	No of data	B (mm)	H (mm)	t (mm)	L (mm)	L/B	E_o (MPa)	$\sigma_{-0.2}$ (MPa)	f_u (MPa)	f_c (MPa)	n	Grade_SS
Lam and Gardner [16]	20	104–110	150–160	2.00–6.02	300	2.96–2.98	183600–202000	251–325	560–721	49.50–61.60	3.20–4.60	Austenitic/304
Yang [53]	17	50.2–150.6	120–200	2.86–7.9	211–400	2.36–2.91	183600–202000	251–325	560–721	49.50–61.60	3.20–4.60	Austenitic/304
Tam et al. [26]	17	50.8–130.80	160–190	1.80–6.3	215–403	2.06–2.93	183700–203000	255–320	532–734	49.50–62.80	3.00–4.50	Duplex/2205
Dai et al. [21]	37	51.3–78.60	110–176	2.80–7.83	200–275	2.36–2.91	183600–202000	251–325	560–721	49.50–61.60	3.20–4.60	Austenitic/316
Rao et al. [61]	22	50.6–200.6	97.90–150.5	3.83–7.80	211–400	2.36–2.91	175000–202000	230–321	564–723	49.50–61.40	3.80–4.30	Duplex/2205
Sanaullah et al. [62]	16	48.2–155.6	50.8–101.00	2.81–7.93	203–404	2.31–2.95	183600–202000	251–325	500–761	49.00–61.70	3.30–5.20	Austenitic/304

Data Availability

The dataset and the ML codes used and developed in our study are available in an online repository in accordance with the owner's data retention policies.

(https://github.com/123Deeptarka/Code-and-Datasets-for-CFSST-columns)

References

[1] Gedge G. Structural uses of stainless steel — buildings and civil engineering. J Constr Steel Res 2008;64(11):1194–8. https://doi.org/10.1016/j.jcsr.2008.05.006.

[2] Fan S, He B, Xia X, Gui H, Liu M. Fire resistance of stainless steel beams with rectangular hollow section: Experimental investigation. Fire Saf J 2016;81:17–31. https://doi.org/10.1016/j.firesaf.2016.01.013.

[3] Gardner L. The use of stainless steel in structures. Prog Struct Eng Mater 2005;7(2):45–55. https://doi.org/10.1002/pse.190.

[4] Uy B, Tao Z, Han L-H. Behaviour of short and slender concrete-filled stainless steel tubular columns. J Constr Steel Res 2011;67(3):360–78. https://doi.org/10.1016/j.jcsr.2010.10.004.

[5] He A, Liang Y, Zhao O. Behaviour and residual compression resistances of circular high strength concrete-filled stainless steel tube (HCFSST) stub columns after exposure to fire. Eng Struct 2020;203:109897. https://doi.org/10.1016/j.engstruct.2019.109897.

[6] He A, Wang F, Zhao O. Experimental and numerical studies of concrete-filled high-chromium stainless steel tube (CFHSST) stub columns. Thin-Walled Struct 2019;144:106273. https://doi.org/10.1016/j.tws.2019.106273.

[7] Tao Z, Uy B, Liao F-Y, Han L-H. Nonlinear analysis of concrete-filled square stainless steel stub columns under axial compression. J Constr Steel Res 2011;67(11):1719–32. https://doi.org/10.1016/j.jcsr.2011.04.012.

[8] Han L-H, Xu C-Y, Tao Z. Performance of concrete filled stainless steel tubular (CFSST) columns and joints: Summary of recent research. J Constr Steel Res 2019;152:117–31. https://doi.org/10.1016/j.jcsr.2018.02.038.

[9] Lai B-L, Zheng X-F, Fan S-G, Chang Z-Q. Behavior and design of concrete filled stainless steel tubular columns under concentric and eccentric compressive loading. J Constr Steel Res 2024;213:108319. https://doi.org/10.1016/j.jcsr.2023.108319.

[10] Standards Australia, Bridge design,part 6: steel and composite construction.

[11] ANSI/AISC 360-16 Specification for Structural Steel Buildings, 2016.

[12] The Department of Housing and Urban–Rural and Development of Fujian Province; 2010, DBJ/T 13-51-2010 Technical Specification for concrete filled structures. Fuzhou (China).

[13] Eurocode 4. Design of composite steel and concrete structures, Part 1.1: General rules and rules for buildings (together with United Kingdom National Application Document). DD ENV 1994–1-1:1994. London W1A2BS: British Standards Institution; 1994. 1994.

[14] He A, Zhao O. Experimental and numerical investigations of concrete-filled stainless steel tube stub columns under axial partial compression. J Constr Steel Res 2019;158:405–16. https://doi.org/10.1016/j.jcsr.2019.04.002.

[15] Lam D, Gardner L. Structural design of stainless steel concrete filled columns. J Constr Steel Res 2008;64(11):1275–82. https://doi.org/10.1016/j.jcsr.2008.04.012.

[16] ACI. 318.Building code requirements for structural concrete., 1995. Detroit: American Concrete Institute; 1995.

[17] Young B, Ellobody E. Experimental investigation of concrete-filled cold-formed high strength stainless steel tube columns. J Constr Steel Res 2006;62(5):484–92. https://doi.org/10.1016/j.jcsr.2005.08.004.

[18] He A, Su A, Liang Y, Zhao O. Experimental and numerical investigations of circular recycled aggregate concrete-filled stainless steel tube columns. J Constr Steel Res 2021;179:106566. https://doi.org/10.1016/j.jcsr.2021.106566.

[19] AS/NZS (Australian/New Zealand Standard). 2017. Composite structures—Composite steel-concrete construction in buildings. AS/NZS 2327-2017. Sydney, Australia: AS/NZS. 2017.

[20] Dai P, Yang L, Wang J, Zhou Y. Compressive strength of concrete-filled stainless steel tube stub columns. Eng Struct 2020;205:110106. https://doi.org/10.1016/j.engstruct.2019.110106.

[21] MOHURD (Ministry of Housing and Urban-Rural Development of the People's Republic of China). Code for design of concrete structures. GB/T 50010-2010, 2010. Beijing: MOHURD; 2010.

[22] Guo L, Liu Y, Fu F, Huang H. Behavior of axially loaded circular stainless steel tube confined concrete stub columns. Thin-Walled Struct 2019;139:66–76. https://doi.org/10.1016/j.tws.2019.02.014.

[23] Li YL, Zhao XL, Raman Singh RK, Al-Saadi S. Tests on seawater and sea sand concrete-filled CFRP, BFRP and stainless steel tubular stub columns. Thin-Walled Struct 2016;108:163–84. https://doi.org/10.1016/j.tws.2016.08.016.

[24] Patel VI, Liang QQ, Hadi MNS. Nonlinear analysis of axially loaded circular concrete-filled stainless steel tubular short columns. J Constr Steel Res 2014;101:9–18. https://doi.org/10.1016/j.jcsr.2014.04.036.

[25] Ding F, et al. Analytical behaviors of concrete-filled circular stainless steel tubular (CFCSST) stub columns under axial loading. Structures 2019;19:277–85. https://doi.org/10.1016/j.istruc.2019.01.013.

[26] Tam VWY, Wang Z-B, Tao Z. Behaviour of recycled aggregate concrete filled stainless steel stub columns. Mater Struct 2014;47(1–2):293–310. https://doi.org/10.1617/s11527-013-0061-1.

[27] Flah M, Nunez I, Ben Chaabene W, Nehdi ML. Machine learning algorithms in civil structural health monitoring: a systematic review. Arch Comput Methods Eng 2021;28(4):2621–43. https://doi.org/10.1007/s11831-020-09471-9.

[28] Adeli H. Neural networks in civil engineering: 1989–2000. Comput -Aided Civ Infrastruct Eng 2001;16(2):126–42. https://doi.org/10.1111/0885-9507.00219.

[29] Nguyen H, Vu T, Vo TP, Thai H-T. Efficient machine learning models for prediction of concrete strengths. Constr Build Mater 2021;266:120950. https://doi.org/10.1016/j.conbuildmat.2020.120950.

[30] Han T, Siddique A, Khayat K, Huang J, Kumar A. An ensemble machine learning approach for prediction and optimization of modulus of elasticity of recycled aggregate concrete. Constr Build Mater 2020;244:118271. https://doi.org/10.1016/j.conbuildmat.2020.118271.

[31] Rahman J, Billah AM, Arafin P, Islam K, Nehdi ML. Design-focused interpretable machine learning models for compressive capacity prediction of gusset plate connections. Eng Struct 2024;298:117038. https://doi.org/10.1016/j.engstruct.2023.117038.

[32] Naderpour H, Mirrashid M, Parsa P. Failure mode prediction of reinforced concrete columns using machine learning methods. Eng Struct 2021;248:113263. https://doi.org/10.1016/j.engstruct.2021.113263.

[33] Asif Bin Kabir Md, Sajid Hasan A, Muntasir Billah A. Failure mode identification of column base plate connection using data-driven machine learning techniques. Eng Struct 2021;240:112389. https://doi.org/10.1016/j.engstruct.2021.112389.

[34] Marie HS, Abu El-Hassan K, Almetwally EM, A. El-Mandouh M. Joint shear strength prediction of beam-column connections using machine learning via experimental results. Case Stud Constr Mater 2022;17:e01463. https://doi.org/10.1016/j.cscm.2022.e01463.

[35] Cakiroglu C, Islam K, Bekdaş G, Isikdag U, Mangalathu S. Explainable machine learning models for predicting the axial compression capacity of concrete filled steel tubular columns. Constr Build Mater 2022;356:129227. https://doi.org/10.1016/j.conbuildmat.2022.129227.

[36] Hou C, Zhou X-G. Strength prediction of circular CFST columns through advanced machine learning methods. J Build Eng 2022;51:104289. https://doi.org/10.1016/j.jobe.2022.104289.

[37] Vu Q-V, Truong V-H, Thai H-T. Machine learning-based prediction of CFST columns using gradient tree boosting algorithm. Compos Struct 2001;259:113505. https://doi.org/10.1016/j.compstruct.2020.113505.

[38] Lee S, Vo TP, Thai H-T, Lee J, Patel V. Strength prediction of concrete-filled steel tubular columns using categorical gradient boosting algorithm. Eng Struct 2021;238:112109. https://doi.org/10.1016/j.engstruct.2021.112109.

[39] F. Pedregosa et al., Scikit-learn: Machine Learning in Python, *Mach. Learn. PYTHON*.
[40] Liang H, Song W. Improved estimation in multiple linear regression models with measurement error and general constraint. J Multivar Anal 2009;100(4):726–41. https://doi.org/10.1016/j.jmva.2008.08.003.
[41] McDonald GC. Ridge regression. WIREs Comput Stat 2009;1(1):93–100. https://doi.org/10.1002/wics.14.
[42] Ranstam J, Cook JA. LASSO regression. 1348–1348 Br J Surg 2018;105(10). https://doi.org/10.1002/bjs.10895.
[43] Myles AJ, Feudale RN, Liu Y, Woody NA, Brown SD. An introduction to decision tree modeling. J Chemom 2004;18(6):275–85. https://doi.org/10.1002/cem.873.
[44] Biau G, Scornet E. A random forest guided tour. TEST 2016;25(2):197–227. https://doi.org/10.1007/s11749-016-0481-7.
[45] Laloë T. A k-nearest neighbor approach for functional regression. Stat Probab Lett Aug. 2008;78(10):1189–93. https://doi.org/10.1016/j.spl.2007.11.014.
[46] Zhang F, O'Donnell LJ. Support Vector Regression. Machine Learning. Elsevier; 2020. p. 123–40. https://doi.org/10.1016/B978-0-12-815739-8.00007-9.
[47] S. Jhaveri, I. Khedkar, Y. Kantharia, and S. Jaswal, Success Prediction using Random Forest, CatBoost, XGBoost and AdaBoost for Kickstarter Campaigns, in *2019 3rd International Conference on Computing Methodologies and Communication (ICCMC)*, Erode, India: IEEE, Mar. 2019, pp. 1170–1173. doi: 10.1109/ICCMC.2019.8819828.
[48] Yang L, Shami A. On hyperparameter optimization of machine learning algorithms: theory and practice. Neurocomputing 2020;415:295–316. https://doi.org/10.1016/j.neucom.2020.07.061.
[49] Fushiki T. Estimation of prediction error by using K-fold cross-validation. Stat Comput Apr. 2011;21(2):137–46. https://doi.org/10.1007/s11222-009-9153-8.
[50] Lubo-Robles D, Devegowda D, Jayaram V, Bedle H, Marfurt KJ, Pranter MJ. Machine learning model interpretability using SHAP values: Application to a seismic facies classification task. SEG Technical Program Expanded Abstracts 2020. Virtual: Society of Exploration Geophysicists; 2020. p. 1460–4. https://doi.org/10.1190/segam2020-3428275.1.
[51] Wang T, Reiffsteck P, Chevalier C, Chen C-W, Schmidt F. An interpretable model for bridge scour risk assessment using explainable artificial intelligence and engineers' expertise. Struct Infrastruct Eng 2023:1–13. https://doi.org/10.1080/15732479.2023.2230564.
[52] AIJ. Recommendations for design and construction of concrete filled steel tubular structures. Tokyo (Japan): Architectural Institute of Japan (AIJ). 2008. 2008.
[53] CSA, Design of Steel Structures (CSA-S16–09), *Can. Stand. Assoc.*, 2009.
[54] Yang B, et al. Mechanical Performance of Circular Ultrahigh-Performance Concrete–Filled Double Skin High-Strength Steel Tubular Stub Columns under Axial Compression. J Struct Eng 2022;148(3):04021298. https://doi.org/10.1061/(ASCE)ST.1943-541X.0003291.
[55] Yan X-F, Hassanein MF, Wang F, He M-N. Behaviour and design of high-strength concrete-filled rectangular ferritic stainless steel tubular (CFFSST) short columns subjected to axial compression. Eng Struct 2021;242:112611. https://doi.org/10.1016/j.engstruct.2021.112611.
[56] Liao F-Y, Hou C, Zhang W-J, Ren J. Experimental investigation on sea sand concrete-filled stainless steel tubular stub columns. J Constr Steel Res 2019;155:46–61. https://doi.org/10.1016/j.jcsr.2018.12.009.
[57] Sener KC, Varma AH. Steel-plate composite walls: experimental database and design for out-of-plane shear. J Constr Steel Res 2014;100:197–210. https://doi.org/10.1016/j.jcsr.2014.04.014.
[58] Thai H-T, Thai S, Ngo T, Uy B, Kang W-H, Hicks SJ. Reliability considerations of modern design codes for CFST columns. J Constr Steel Res 2021;177:106482. https://doi.org/10.1016/j.jcsr.2020.106482.
[59] Galambos TV. Load and resistance factor design. Eng J 1981.
[60] Kazemzadeh Azad S, Li D, Uy B. Compact and slender box concrete-filled stainless steel tubes under compression, bending, and combined loading. J Constr Steel Res 2021;184:106813. https://doi.org/10.1016/j.jcsr.2021.106813.
[61] Rao L, Yue Q, Huang B, Liu X. Axial compressive performance of novel square coral concrete-filled duplex stainless steel tubes. J Build Eng 2022;49:104068. https://doi.org/10.1016/j.jobe.2022.104068.
[62] Ri Q, Dqg F. Behavior of concrete filled stainless steel tubular. COLUMN Axial Loads 2019;7(1).